https://doi.org/10.5194/acp-2021-172
Preprint. Discussion started: 9 March 2021

Atmospheric Chemistry and Physics Discussions

Changes of cirrus cloud properties and occurrence over Europe during the COVID-19 caused air traffic reduction

Qiang Li[1] and Silke Groß[1]

[1]Deutsches Zentrum für Luft- und Raumfahrt, Institut für Physik der Atmosphäre, D-82234 Oberpfaffenhofen, Germany,
Correspondence to: Qiang Li (qiang.li@dlr.de) and Silke Groß (silke.gross@dlr.de)

Abstract. By inducing linear contrails and contrail cirrus, air traffic has a main impact on the ice cloud coverage and occurrence. During the COVID-19 pandemic the civil air traffic over Europe was significantly reduced: in March and April 2020 to about 80% compared to the year before. This unique situation allows to study the effect of air traffic on cirrus clouds. This work investigates based on satellite lidar measurements if and how cirrus cloud properties and occurrence changed over Europe in the course of COVID-19. Cirrus cloud properties are analyzed for different years, which showed similar meteorological conditions for March and April as they were found for 2020. Comparing these years shows that the cirrus cloud occurrence was reduced by about 30% with smaller cloud thicknesses found in April 2020. The average thickness of cirrus clouds was reduced to 1.18 km in April 2020 compared to a value of 1.40 km under normal conditions. In addition, the cirrus clouds measured in April 2020 possess smaller mean values of the particle linear depolarization ratio (PLDR) than the previous years at a high significance level, especially at colder temperatures (T < -50°C). The same exercises are extended to the observations over the United States of America and over China. Besides the regional discrimination of cirrus clouds, we reach the final summary that cirrus clouds show significant changes of depolarization ratios in both March and April over Europe, no changes in both months over China, and significant changes only in April over USA.

1 Introduction

Cirrus clouds have a wide global coverage and thus a large effect on the Earth's radiation budget. It is assumed that mid-latitude cirrus clouds in general have a warming effect (*Chen et al.*, 2000), but their radiative effects strongly depend on their microphysical properties, e.g. particle number concentration, size, and shape (e.g. *Stephens et al.*, 1990; *Haag and Kärcher*, 2004). Ambient conditions, like temperature and supersaturation (e.g. *Heymsfield*, 1977; *Khvorostyanov and Sassen*, 1998), but also the nucleation mode (e.g. *Ström and Ohlsson*, 1998; *Seifert et al.*, 2004; *Urbanek et al.*, 2018) can influence the microphysical properties of the cirrus clouds. Previous studies reveal that ice crystals in air form and grow as a function of temperature and ice supersaturation and there is a general trend toward larger morphological complexity as the supersaturation increases as well as the temperature drops (e.g. *Heymsfield*, 2003; *Bailey and Hallett*, 2009). Based on laboratory experiments, Bailey and Hallett (2004) reported that different ice crystal habits were observed under conditions with different temperatures. The natural ice crystals, however, which encounter varying temperature and humidity may grow into irregular forms (*Korolev et al.*, 1999). Furthermore, mass transport (including convection and advection) and crystal origin at a sample region also

https://doi.org/10.5194/acp-2021-172
Preprint. Discussion started: 9 March 2021


Atmospheric Chemistry and Physics Discussions

govern the correlation between temperature and ice crystal habits (e.g. *Bailey and Hallett*, 2004; *Um et al.*, 2015). Differences in size and shape have an impact on the particles' optical properties; it was found that columnar ice crystals generate higher depolarization ratios than plate-like crystals (*Noel et al.*, 2006), with the highest lidar depolarization ratios found for irregularly shaped ice crystals.

According to theoretical ray-tracing simulations of laser backscatter depolarization (e.g. *Takano and Liou*, 1989), the geometric properties (shape and composition) of aerosols and ice crystals have a strong influence on the scattering characteristics of light. Light scattering by atmospheric ice crystals lead to a change of polarization according to the internal ray paths, more precisely, increasing with increasing hexagonal axis ratio (= length over width). The particle linear depolarization ratio (PLDR) used to evaluate this effect is a well-defined parameter to retrieve information on ice crystal habits in terms of particle phase, shape, and orientation. The lidar transmits linearly polarized light into the atmosphere. The light scattered in backward direction by spherical particles has the same orientation of polarization as the incident light, whereas non-spherical particles such as cirrus ice crystals can display different polarization states according to their shape and size distribution (*Sassen et al.*, 1989; *Freudenthaler et al.*, 2009; *Urbanek et al.*, 2018). The polarization lidar technique is a well-established and widely-used method to provide information on aerosol profiling and to distinguish between different types of aerosols, e.g. non-spherical mineral dust particles with high values of the PLDR (*Freudenthaler et al.*, 2009; *Tesche et al.*, 2009; *Groß et al.*, 2012). It is also used to unambiguously differentiate between ice clouds and water clouds (e.g. *Bühl et al.*, 2016) and to study the characteristics of ice clouds (e.g. *Schotland et al.*, 1971; *Sassen*, 1991; *Ansmann et al.*, 2003; *Groß et al.*, 2012; *Urbanek et al.*, 2018). The basic product of a polarization lidar is the volume linear depolarization ratio δ which is defined as the ratio of the returning light power from polarization components perpendicular (cross-polarized) and parallel (co-polarized) to the polarization direction of the transmitted laser source. It includes the scattering of molecules and particles and is thus dependent on particle concentration. In contrast, the particle linear depolarization ratio, defined as the ratio of the perpendicular and parallel component of the backscatter coefficient, characterizes only the scattering properties of particles. It is independent from their concentration and can be used to characterize differences in particle properties. PLDR is a key parameter that is commonly used in the lidar field to quantify the changes in polarization and to retrieve information on ice habit in clouds (e.g. Sassen and Zhu, 2009). Using the measurements of an airborne lidar during the ML-CIRRUS campaign 2014 over Europe (*Voigt et al.*, 2017), *Urbanek et al.* (2018) found enhanced values of the PLDR of cirrus clouds forming in areas of high aviation emissions. They interpreted these changes as an effect of more frequent heterogeneous freezing on aviation exhaust particles. It has long been known that aircraft-emitted particles may act as efficient ice nuclei leading to heterogeneous nucleation in regions with a favorable atmospheric state (including temperature and humidity) (e.g. *Schumann*, 1996; *Jensen and Toon*, 1997; *Kärcher*, 2007). Further, aviation-induced aerosols and contrails can alter the properties of cirrus clouds (e.g. *Tesche et al.*, 2016; *Kärcher*, 2017; *Urbanek et al.*, 2018). This region was also used in a recent study by *Schumann et al.* (2021) to investigate air traffic and contrail changes during COVID-19. They found that the reduced contrail length for a 6-month period (March-August) in 2020 was caused only partly by air traffic reduction and partly by less favourable meteorological conditions. To largely exclude the effect of meteorological conditions on cirrus occurrence and cirrus properties in our study, we extended this study to a larger

https://doi.org/10.5194/acp-2021-172
Preprint. Discussion started: 9 March 2021


Atmospheric Chemistry and Physics Discussions

number of years but focused only on March and April measurements as they showed the least differences for the different years and the strongest reduction in air traffic.

During the COVID-19 pandemic aviation was significantly reduced over Europe. Eurocontrol reports a drop of more than 80% beginning mid of March 2020, with its peak of -88% in April 2020 (source: www.eurocontrol.int/covid19). Since May/June 2020 aviation shows a slight recovery to about 40-50% of air traffic compared to the year before. Thus, this episode provides a unique testbed to investigate changes in cirrus cloud properties and occurrence due to reduced aviation. In our study we use spaceborne lidar measurements from the CALIPSO satellite (*Winker et al.*, 2010) to study cirrus cloud properties over the European region. We focus on this area as an impact on cirrus cloud properties from aviation induced aerosols was found for this region (*Urbanek et al.*, 2018).

In Section 2 we will outline the CALIPSO data and methods. Section 3 describes our results concerning changes of cirrus cloud properties and occurrence in April 2020 compared to three reference years (2014, 2017 and 2019) with similar meteorological situations as in 2020. A discussion of our findings, including a significance test, is given in Section 4. And finally, Section 5 concludes this work.

2 Data and Methods

The Cloud-Aerosol Lidar and Infrared Pathfinder Satellite Observation (CALIPSO) satellite was launched on April 28, 2006 and is flying as part of the NASA Afternoon Constellatin or A-Train in a sun-synchronous polar orbit at an altitude of 705 km with an equator-crossing time of about 1:30 PM and a 16-day repeat cycle (*Winker et al.*, 2010; *Stephens et al.*, 2018). Since September 2018, CALIPSO has moved to a lower orbit (16.5 km lower than the A-Train) to join the CloudSat satellite in orbit to simultaneously probe the Earth system. The main objectives of CALIPSO mission are to provide information on the vertical distributions of aerosols and clouds as well as their physical properties over the globe with unprecedented spatial resolution which is beneficial to complement current measurements and to improve our understanding of weather and climate. The Cloud-Aerosol Lidar with Orthogonal Polarization (CALIOP) instrument is the primary payload along with an Imaging Infrared Radiometer (IIR) and a Wide-Field Camera (WFC) carried on the CALIPSO satellite. CALIOP is a dual-wavelength polarization lidar system with a three-channel receiver, optimized for global profiling of aerosols and clouds and their optical and microphysical properties. CALIOP is built around a diode-pumped Nd:YAG laser which produces simultaneous co-aligned pulses at 532 nm and 1064 nm (*Winker et al.*, 2007; *Hunt et al.*, 2009). Each laser produces 110 mJ energy at each of the two wavelengths per pulse with a repetition rate of 20.16 Hz (corresponding to a horizontal resolution of 333 m on the Earth's surface). The augular divergence of each laser beam is reduced to approximately 100 μrad thanks to the beam expander on each laser, which results to a footprint of 70 m diameter on the Earth's surface. Backscattered signals are received by a 1-m telescope, which feeds a three-channel receiver. The 1064-nm receiver channel is polarization insensitive and only measures the elastic backscatter intensity. While two polarization-sensitive 532-nm receiver channels independently measure two orthogonal polarization components which are polarized parallel and perpendicular to the polarization plane of the transmitted beam. Since

https://doi.org/10.5194/acp-2021-172
Preprint. Discussion started: 9 March 2021


Atmospheric Chemistry and Physics Discussions

the launch of CALIPSO, numerous validation studies have been carried out with ground-based (e.g. *Pappalardo et al.*, 2010; *Mamouri et al.*, 2009; *Lopes et al.*, 2013) and airborne (e.g. *McGill et al.*, 2007; *Burton et al.*, 2013) lidar measurements.

The CALIPSO data used in this study are the Level 2 5-km Cloud Profile Products which contain the information of scientific parameters such as particle linear depolarization ratio, temperature (derived from the GEOS-5 data), ice water content (derived from the CALIOP retrieved extinction by ice cloud particles) etc. The CALIOP data are stored as half orbits from north to south and thereby separated by day and night. Daytime observations are affected by solar background illumination that decreases the signal-to-noise ratio, making the daytime measurements more challenging to interpret. However, in the north Atlantic flight corridor covering the European region which we are interested in, there is an aviation fingerprint with two maxima during morning eastbound and afternoon westbound traffic (e.g. *Graf et al.*, 2012; *Schumann and Graf*, 2013). In the current study, therefore, all measurements (both daytime and nighttime) will be analyzed in order to study the influence of air traffic on cirrus clouds to the fullest extent.

CALIOP has a fundamental sampling resolution of 30 m vertical and 335 m (1/3 km) horizontal, depending on the receiver electrical bandwidth and the laser pulse repetition rate. However, the spatial scales of atmospheric variability tend to increase with altitudes and the backscatted signals from particles (such as clouds and aerosol layers) above that from ambient air molecules become weaker. To overcome this situation, CALIOP has conducted different averaging algorithms for different altitudes for a better detection of occurring features in the atmosphere (*Vaughan et al.*, 2009; *Winker et al.*, 2009), which allows to retain the fundamental vertical resolution of 30 m in the lower troposphere and to identify the fainter features with required signal-to-noise ratio in the high altitudes. The details of the spatial resolutions of the CALIOP data are listed in Table 1.

The fundamental measurements made by CALIOP are calibrated altitude-resolved profiles of backscatter intensity from a variety of geophysical entities, including clouds, aerosol layers, regions of clear air, and the returns from the Earth's surface. Retrievals of aerosol and cloud properties and the correct interpretation of their measurements require first the accurate discrimination between aerosols and clouds within the observed profilings. Furthermore, cloudiness comsisting of a variety of cloud types are characterized by different optical and physical properties and have different influence on radiative forces and precipitation. The CALIPSO team developed the vertical feature mask (VFM) to classify aerosols and clouds based on statistical differences in the various optical and physical properties of the detected layers and further to separate them into different subtypes (e.g. *Liu et al.*, 2004, 2009; *Hu et al.*, 2009; *Omar et al.*, 2009; *Vaughan et al.*, 2009). The VFM products stored also in the Level 2 data are used in this study to distinguish cirrus clouds from aerosols and non-cirrus clouds.

A cloud layer product of CALIPSO includes cloud different properties: e.g. cloud height, backscatter, extinction, ice/water phase. In order to exclude misclassified mix-phased clouds and noise-contaminated signals, we only consider measurements at temperatures below -38°C (=235 K), above 6 km altitudes and with cloud thickness larger than 0.1 km. The observations of cirrus clouds with CALIPSO are used to infer cirrus occurrence rates (OR). This analysis is carried out on single cirrus cloud profiles (determined with VFM) grouping the cirrus clouds in geometrical thicknesses of 100 m, 300 m, 1 km, and 2 km, respectively. The cirrus OR are hence calculated as the ratio of the number of profiles with cirrus cloud layers to the total number of observed profiles. In order to compare the changes of cirrus occurrence and properties under the conditions of reduced air traffic, we consider statistical values of the cirrus OR (here monthly mean) rather instead of single cases.

https://doi.org/10.5194/acp-2021-172
Preprint. Discussion started: 9 March 2021


Atmospheric Chemistry and Physics Discussions

Table 1. Spatial resolution of downlinked data from CALIOP at 532 nm

Altitude range (km)	Horiztontl resolution (km)	Vertical resolution (m)
30.1–40.0	5.025	300
20.2–30.1	1.675	180
8.2–20.2	1.005	60
-0.5–8.2	0.335	30

It is mentioned above that CALIPSO provides global measurements of cloud profilings in the troposphere and lower stratosphere. In this study, however, we have concentrated on the similar area as the ML-CIRRUS campaign (*Voigt et al.*, 2017), more precisely, the whole range of the midlatitudes from 35°N to 60°N and from the Atlantic ocean (15°W) to central Europe (15°E) (for the sake of simplicity, we call the here-considered area as Europe in the rest of this manuscript). As CALIOP is a nadir-pointing lidar, data is collected only along the ground track of the CALIPSO satellite. CALIPSO flies 3-4 times each day over this area and therefore ∼100 tracks of observations each month were collected in March and April. Further, this area covers a large fraction of the North Atlantic flight corridor connecting central Europe with north America where the generation of contrail-induced cirrus clouds and the aviation impact on cirrus clouds have been intensively studied (e.g. *Graf et al.*, 2012; *Schumann and Graf*, 2013; *Voigt et al.*, 2017; *Urbanek et al.*, 2018; *Schumann et al.*, 2021).

3 Results

Cirrus ice crystals generally form in the outflow frontal of the deep convections and in the regions of ascending motions (producing the supersaturation of ice), or they form by ice nucleation on aerosol particles in the upper troposphere. Aircraft emission of aerosols can lead to the formation of contrails depending on the surrounding meteorological conditions (including temperature, pressure, and humidity) of the flight track. After formation, contrails can further spread out as persistent contrails and develop into contrail cirrus clouds when the background air is supersaturated with respect to ice. In addition, the aerosols might also change the optical properties of naturally occurring cirrus clouds. To exclude that changes found in ice cloud occurrence and properties are caused by substantial differences in meteorological conditions we analyze monthly/bi-monthly climate composites of geopotential height (GPH) at 500 hPa (as measure for the general circulation pattern), temperature and humidity for the region covering the extra-tropical North Atlantic and the European mainland. For this analysis National Center for Environmental Predictions/National Center for Atmospheric Research (NCEP/NCAR) Reanalysis 1 (e.g. *Kalnay et al.*, 1996; *Kistler et al.*, 2001) are applied. The corresponding data can be achieved through Physical Sciences Laboratory, NOAA, Boulder, Colorado, from their website at https://psl.noaa.gov/. We found a general good agreement for the circulation pattern (see GPH at 500 hPa in Figure 1) as well as for the temperature (at the surface and at 850 hPa which are not shown here) for the March and April of 2014-2019 compared to 2020. Looking at the year to year variability in 2016 and 2018 showed slight differences with a stronger component of northwesterly flow in the western part of our observation area for 2016 and an

https://doi.org/10.5194/acp-2021-172
Preprint. Discussion started: 9 March 2021

Atmospheric Chemistry and Physics Discussions

Table 2. The temperature and humidity of the background in the altitude ranges 8-13 km derived from the GEOS-5 model data product which is provided to the CALIPSO by the GMAO data assimulation system.

	Temperature (°C)		Rel. humidity (%)	
Year (April)	Medain	Mean	Median	Mean
2014	-50.997	-50.142	95.119	90.020
2015	-51.803	-51.206	95.224	90.513
2016	-49.712	-49.890	95.902	88.993
2017	-52.639	-52.150	95.473	90.382
2018	-50.644	-50.172	96.604	91.659
2019	-51.342	-50.737	96.655	91.703
2020	-51.539	-50.712	96.718	91.725

eastward shift of the general situation pattern in the observation area for 2018. However, looking at the year to year variability for the time period May-August we conclude that the general meteorological conditions might have a quite large impact on weather and cloudiness in the observation area. Thus we confine our study to March and April data. For the relative humidity we found that the relative humidity for those ranges shows quite a wide regional dependence. The largest agreement of the general situation in March/April 2020 is found for 2014. Looking at the median and mean values of the general distribution we conclude that 2020 is well comparable to former years. Unfortunately, the reanalysis data only include the relative humidity over water and only up to 300 hPa. To overcome this and for a more precise evaluation of our measurement area, we used the temperature and humidity data derived from the GEOS-5 (Goddard Earth Observering System, Version 5) model data product provided to the CALIPSO by the GMAO data assimulation system. For those analysis we only focused on the specific altitudes within the range between 8 and 13 km. The derived temperature and humidity along with their median and mean values in April are shown in Figure 2. The relative humidity shows median (mean) values from 95.1% to 96.7% (from 89.0% to 91.7%) (see Table 2 for the median and mean values of temperature and humidity in different years). With the values for 2020 being at the uppermost part of the distribution, however, they are about the same as for April 2015, 2018, 2019, and only slightly larger than for 2014 and 2017. 2016 shows the lowest value. With a mean value of only 89.0% it is the driest year in our consideration. Looking at the median and mean values of the temperature in the considered height ranges for the different years, we see a larger spread as found for the relative humidity. However, the values differ in a range of about 3°C. With a median (mean) value of about -51°C (∼-50°C) 2020 is quite comparable to the conditions in 2014, 2015, and 2019. 2017 showed slightly lower temperatures with a median (mean) value of about -53°C (about -52°C). The highest median/mean value is found for 2016 and 2018. It was about 1-2°C larger than found for the other years. To exclude that the differences in the meteorological propierties may impact our results we mainly focus our analysis to the years 2014, 2017, 2019 and 2020. So, we use CALIPSO data of March and April to investigate changes in the cirrus cloud occurrence and properties caused by reduced aviation.

https://doi.org/10.5194/acp-2021-172
Preprint. Discussion started: 9 March 2021

Atmospheric Chemistry and Physics Discussions

Table 3. The occurrence rates of cirrus clouds with the definition based on different geometrical cloud thicknesses shown in Figure 3 as well as the results in April of years 2015, 2016, and 2018.

	Cirrus occurrence rate (%)			
Year (April)	> 0.1 km	> 0.3 km	> 1.0 km	> 2.0 km
2014	32.1	29.0	16.6	5.0
2015	34.5	32.1	20.5	7.1
2016	19.1	16.6	9.2	2.8
2017	33.9	30.0	17.5	5.8
2018	32.2	29.4	17.0	5.1
2019	31.4	28.3	16.9	6.0
2020	24.8	21.8	12.0	4.0

3.1 Occurrence rate and cloud thickness

Resulting histograms of the cirrus occurrence rate (OR) in April for the different years are shown in Figure 3. The research area (35°N–60°N and 15°W–15°E) we use for our study is indicated by the red box on the map (see left panel of Figure 3). For all years considered in this study the OR profiles show the maxima at the altitude of about 9.5 km. However, cirrus clouds in 2020 show a reduced OR of only about 9.5% compared to about 11.5% in the reference years. In general, cirrus clouds were found in a height range of 6-14 km, where the cirrus OR for 2020 shows a clear reduction in the height range from about 7 to about 12 km compared with the reference years. The profiles of cirrus OR for the three reference years show almost no variation. Even if we extend our examination (not shown) to the years 2015 we do not see a difference in the profiles of cirrus OR compared to the reference profiles. And even for 2018 the profile of cirrus OR differes only in larger altitude regions from the other reference years. However, the cirrus OR profile for April 2016 shows a clear reduction due to the meteorological conditions (warmer and dryer airmasses). Comparing the profiles of cirrus OR for March (not shown) we found similar conditions also for 2016. I.e., we see no apparent differences of the OR profiles for the years 2014-2017 and 2019 but a clear reduction of OR for 2020. 2018 (March results) shows the behaviour similar to April with a reduction only in the uppermost altitude ranges compared to all other years. The cirrus OR depends on the geometrical thickness of the cloud (see the right panel of Figure 3). The largest reduction in cirrus OR in 2020 is found for geometrical thicknesses of 0.1 km, 0.3 km and 1.0 km, with an OR of 25%, 22%, 12%, respectively. The reference years show values of >31%, >28%, and >16%, respectively. The cirrus OR for a geometrical thickness of 2.0 km shows only minor reduction of overall about 4% compared to more than 5% of the reference years. The exact OR values for the different cirrus cloud geometrical thicknesses are given in Table 3. From the current analysis, it is striking to note that the cirrus OR in April 2020 are smaller by a factor of 30% than the values derived in the reference years in despite of the cloud thicknesses on which a cirrus cloud was defined. The same findings, although with a smaller proportion, are also seen in the observations of March 2020 (not shown). Our results are consistent with the previous findings that air traffic might increase the occurrence of cirrus clouds (*Boucher*, 1999).

https://doi.org/10.5194/acp-2021-172
Preprint. Discussion started: 9 March 2021


Atmospheric Chemistry and Physics Discussions

We next turn to a comparison of the geometrical thickness of cirrus clouds which is defined as the vertical extension of cirrus clouds; no matter how many layers the clouds can be characterized by (i.e., either the clouds are continually distributed or not). In the analysis, cirrus clouds with thickness smaller than 0.1 km are considered as cirrus free and the corresponding observations will be neglected. The calculated occurrence frequencies of the cirrus thicknesses from the observations in April are shown in the histograms (bar width of 0.2 km) in Figure 4. From all the here-analyzed observations, the distributions of the cirrus thicknesses are positively-skewed with a long tail extending to larger values up to ∼5 km. There are maximum occurrence frequencies found to fall within the range of 0.1–1.5 km. The decrease of occurrence frequencies of cloud thickness towards larger values is much sharper from the results in 2020 than in other years. The calculated average thicknesses are 1.43, 1.37, and 1.42 km in April of the years 2014. 2017, and 2019, respectively, which are in good agreement with the typical value of cirrus thickness of 1.5 km reported by previous studies (e.g. *Dowling and Radke*, 1990). The average thickness of cirrus clouds in April 2020, however, is significantly smaller and reduced to only 1.18 km.

3.2 Particle linear depolarization ratio

We next compare the relation between the cirrus PLDR with the corresponding ambient temperatures of different years. The determined relations are shown in Figure 5 where a heatmap coloring is used to specify the number density of the scatter point data. First of all, there are hot spots (with a large amount of data points) found for all cases at the temperatures higher than ∼-45°C where PLDR mostly fall into a range between ∼0.20 and 0.55. This hotspot is similar for all the analyzed years. We further note that there is a secondary hot spot within the temperature range of -60°C to -50°C with larger PLDR of up to 60% in the years 2014, 2017, and 2019. Less cirrus clouds, however, were detected at this lower temperature range (<-50°C) in 2020. In addition, at temperatures higher than -50°C there are no clear correlations found between PLDR and temperatures. At -50°C and colder, however, there is a clear negative correlation between PLDR and temperatures, namely that cirrus PLDR increase with falling temperatures which agrees with many previous cirrus observations (e.g. *Sassen and Benson*, 2001; *Urbanek et al.*, 2018).

In order to further clarify this feature, we divide the data into a subset for temperatures from -38°C to -50°C and colder than -50°C. T = -50°C is one of the threshold conditions for contrail formation (*Schumann*, 1996). Before going into details, it is important to mention that the PLDR values below 0.10 and above 0.80 were cut off, for the consideration that those values are correlated with large uncertainties and should be unphysical. Resulting histograms of cirrus PLDR and their median values for the different temperature regimes are shown in Figure 6. First of all, the histograms of cirrus PLDR can be characterized by a right-skewed distribution with a long tail extending to larger values. The distributions of PLDR show that in general the PLDR values at lower temperatures (<-50°C) are larger than at higher temperatures (>-50°C), namely that the distributions of PLDR at lower temperatures have a larger skewness to the right (larger values). Focusing in more details on the comparisons, however, we note that the distributions of PLDR at higher temperatures are in good agreement for all the cases with median values of 0.344, 0.344, 0.354 and 0.330 for the years 2014, 2017, 2019 and 2020, respectively. While the PLDR at temperatures colder than -50°C show a significant reduction in 2020 compared to the reference years. The medians of cirrus PLDR for the years 2014, 2017 and 2019 are quite similar with values of 0.392, 0.394 and 0.391, respectively. The median of the cirrus PLDR for

https://doi.org/10.5194/acp-2021-172
Preprint. Discussion started: 9 March 2021


Atmospheric Chemistry and Physics Discussions

2020, however, is only 0.360 at temperatures <-50°C. As, besides the dependence on the temperature, the PLDR might also depend on an aviation effect, it should also be visible for the different meteorogical condistions. Thus, we also looked at the yeas 2015, 2016 and 2018 (not shown) and find median values of 0.390, 0.400, and 0.378 at temperatures lower than -50°C and of 0.334, 0.356, and 0.347 at higher temperatures (>-50°C), respectively. This feature of PLDR can be interpreted by the fact that the contrails which may lead to contrail-induced cirrus characterized by higher PLDR were observed at temperatures below around -50°C (e.g. *Schumann*, 1996; *Voigt et al.*, 2011) in the normal years, whereas lack of contrails due to the reduction of air traffic in April 2020. In addtion we note that the cirrus clouds in April 2016 were characterized by signicantly reduced occurrence rates due to warmer and drier airmasses, while their PLDR were comparable to the other reference years.

We also compare the vertical profiles of the PLDR median (Figure 7 - solid lines) along with the corresponding 20% and 80% percentiles (dashed lines) for the height range between 8 and 12.3 km. These are the typical cruising altitudes for passenger and cargo aircrafts. The resulting profiles of PLDR show a well-known increase with increasing altitudes (e.g. *Urbanek et al.*, 2018) for all the cases. However, the median values of the cirrus cloud's PLDR profile in 2020 is reduced to only about 0.31 at 8.5 km and about 0.38 at 11.5 km compared to median values of about 0.34 at 8.5 km to 0.41 at 11.5 km for the other three years. Despite these reduced values the profile of the April 2020 data shows the same behavior (altitude dependence) as the previous years. The similar feature was found for the March measurements (not shown here). But the decreases of the PLDR with height were only found at altitudes larger ∼10 km in 2020. We should mention that the reduction of air traffic over Europe started from the beginning of March, e.g., air traffic over Germany reduced to about 40% on March 17 and to 80% on March 25, and remained in entire April.

4 Discussion

Our analysis above shows that comprehensible and precise reductions were found in the occurrence rates and thicknesses of cirrus clouds during the period of coronavirus pandemic in March and April, 2020, when the public air traffic was significantly reduced (more than 80% in entire April). Before we may draw final conclusions on the findings, a significance test and parallel comparisons with other regions will be further carried out.

It is mentioned above that the derived PLDR of cirrus clouds are not normally distributed. In order to test the significance of difference between the cirrus PLDR in different years, we here applied a Mann-Whitney U test which is a widely-used nonparametric test for equality of variable medians of two independent samples. Before taking the exercise, we have to down-sample the data since the datasets have a huge number of data points. The sampling has been done for a function varying in time at the same altitude with a sampling rate of 1/10, i.e., one data point was sampled from every 10 points, although the data set after sampling still have more than 20 thousand data points. Comparisons between the sampled data and the corresponding original data in different years have also been done, respectively, showing the same (or a similar) distributions with a high significance level. The overall results of the Mann-Whitney U test with a significance level of p = 5% are presented in Tables 4 and 5. For the observations in March, it is striking that the distributions of cirrus PLDR in the years of 2014, 2017, and 2019 are significantly the same (with p > 5%). While the resulting PLDR in 2020 are significantly different from the previous years

https://doi.org/10.5194/acp-2021-172
Preprint. Discussion started: 9 March 2021


Atmospheric Chemistry and Physics Discussions

(p = 0). In April, we see the 2020 results are again significantly different from the other years and the PLDR distribution in 2017 and 2019 are nearly the same (p = 95.6%). However, the distribution of PLDR in 2014 are slightly different from the results in 2017 and 2019, although the p-values are larger than 1%.

https://doi.org/10.5194/acp-2021-172
Preprint. Discussion started: 9 March 2021

Atmospheric Chemistry and Physics Discussions

Table 4. Significance test using Mann-Whitney U test: March, Europe

year	2014	2017	2019	2020
2014	p= 1, h = 0	p = 0.3356, h = 0	p = 0.3537, h = 0	p = 5.46e-21, h = 1
2017		p = 1, h = 0	p = 0.0618, h = 0	p = 4.10e-26, h = 1
2019			p = 1, h = 0	p = 2.48e-17, h = 1
2020				p= 1, h = 0

Table 5. Significance test using Mann-Whitney U test: April, Europe

year	2014	2017	2019	2020
2014	p= 1, h = 0	p = 0.0244, h = 1	p = 0.0118, h = 1	p = 2.34e-82, h = 1
2017		p = 1, h = 0	p = 0.9560, h = 0	p = 7.58e-69, h = 1
2019			p = 1, h = 0	p = 1.27e-78, h = 1
2020				p= 1, h = 0

It is mentioned in Introduction that the periods of coronavirus pandemic in different regions are different. It provides us a great opportunity to compare the properties of cirrus clouds detected at different regions to study how the reductions of air traffic influence on the cirrus clouds and what the response time of the changes are. For the locations of the study regions we concentrated on Europe (Latitude: 35°N–60°N; Longitude: 15°W–15°E), China (Latitude: 20°N–45°N; Longitude: 90°E–130°E), and the United States of America (Latitude: 30°N–50°N; Longitude: 125°W–75°W), respectively. All the regions are located within the midlatitudes. First of all, the occurrence rates (OR) of cirrus clouds over these three regions show that on average the cirrus clouds occurred more frequently over Europe and USA than over China. This findings show overall agreement with previous studies (e.g. *Sassen et al.*, 2008). Furthermore, we see the same changes in the cirrus OR in April over USA as over Europe but no clear changes in March over USA. For China we found no changes at all for the March and April data.

We next turn to compare the cirrus PLDR in different regions. The same pre-analysis as described above were also carried out, namely that only the observations with the PLDR values between 0.10 and 0.80 and at altitudes between 8 and 12.3 km are considered. The corresponding results over Europe, USA, and China, are shown in Figure 8. The boxes (in black) represent 25th–75th percentiles of all the PLDR values showing the middle 50% of the data (i.e., box bottom stands for the lower quartiel and top for the upper quartile). The medians representing the mid-point of the data set are shown by the red lines through the corresponding boxes and the means are shown by the red circles. For all the cases, the PLDR possess a larger mean than the corresponding median, indicating that the distributions of the PLDR are positively skewed as has been reported above. The box plots provide a general picture of the determined PLDR of cirrus clouds over these three regions. Focusing on the results of Europe, we see the same properties of cirrus clouds as stated above, namely that the cirrus PLDR show excellent agreement

https://doi.org/10.5194/acp-2021-172
Preprint. Discussion started: 9 March 2021


Atmospheric Chemistry and Physics Discussions

with each other in the years 2014, 2017, and 2019 whereas reduced values in 2020 in both months. Further, the reduction of the PLDR in March is slightly smaller than that in April, which should be somehow correlated with the different periods with reduced air traffic in March and April over Europe. We next focus on the results observed over USA and see slightly larger values in 2017 for both months which may be due to the variations of meteorological conditions in different years and is comprehensible. Besides this point, we stress that the PLDR values in 2020 show no clear reduction in March but a significant reduction in April, which is expected because the outbreak of coronavirus in USA started slightly later than in Europe and the domestic flights were sharply reduced in April started later than in Europe. From the observations over China, there are no clear reductions found in 2020 in both months. This is likely due to the facts that the slow recovery in China has started since March and the domestic flights in China are less frequent than in Europe and USA. As for the smaller values of PLDR in April 2014 over China, we checked the altitude profiles of cirrus occurrence and found that most of cirrus clouds in this month occurred at lower altitudes by a factor of $\sim$1 km than other cases (not shown here).

In addition to the different outbreak times of the coronavirus pandemic in different regions, it is important to note that Europe and USA are located more within the aviation corridors than China (e.g. *Stettler et al.*, 2013) and hence the formation and properties of cirrus clouds over Europe and USA are under more impacts by the air traffic. The reduction of air traffic during the pandemic may lead to larger changes in cirrus clouds over Europe and USA than over China. The cirrus PLDR derived over China show on average smaller values than over Europe and USA with the middle 50% (see the boxs in Figure 8) covering a narrower range of PLDR ($\sim$0.03–0.04 less). While the PLDR of cirrus clouds over the latter two regions are in good agreement with each other. This feature further strengthens the assumption that air traffic does not have a major impact on cirrus cloud coverage and properties over China. Due to the westerly jet stream, aerosol source is dominated by clean marine for the north Atlantic and European region and for the north American region, whereas by continental and dust for the Chinese region.

5 Conclusions

The abrupt outbreak and rapid spread of the coronavirus disease (COVID-19) pandemic have become a global public health crisis. In order to curb the spread of the pandemic, most, if not all, governments worldwide have carried out containment measures including lockdowns, quarantines, curfews and restriction of public air traffic as well. In the current paper, we have presented the ocurrence rates, thicknesses and PLDR values of cirrus clouds observed by the space-borne lidar CALIOP on the CALIPSO satellite over the north Atlantic and the European mainland during the period of coronavirus pandemic with reduced public air traffic in 2020. The results have been compared with the corresponding observations in different other years, not affected by air traffic reduction. Cirrus clouds have been retrieved using the VFM products along with additional filters including a temperature mask ($T < -38^{\circ}C$), height threshold ($h > 6$ km), and cloud thickness threshold (> 0.1 km).

Resulting altitude profiles of the cirrus occurrence rates show that cirrus clouds occurred mostly within the altitude range between 7 and 13 km with the maximum occurrence at $\sim$9.5 km in every year (in March and April) here considered. Besides this general agreement, the cirrus occurrence rates show reduced values in 2020. In addition, clear departures of the cirrus

https://doi.org/10.5194/acp-2021-172
Preprint. Discussion started: 9 March 2021


Atmospheric Chemistry and Physics Discussions

occurrence in 2020 from the reference years are found within the height range of 8–12 km in which most public air traffics take place. The same features were also seen in the comparisons of cirrus occurrence rates determined according to different definitions of cirrus clouds as a funciton of cloud thickness, namely that the cirrus clouds in April 2020 occurred less frequently by a factor of 30% than the corresponding periods in the referece years in despite of the cloud thickness used to define a cirrus cloud. The thicknesses of cirrus clouds have further been determined and their histograms can be charaterized by a right-skewed distribution with maximum occurrence frequencies between 0.1 and 1.5 km as well as with a much sharper decrease towards larger values in 2020 compared with other yeras. For the calculated average thicknesses, the results show a much smaller value of only 1.18 km in April 2020 compared with approximately 1.40 km in the previous years.

Turning next to a comparison of the PLDR of cirrus clouds, we divide the data into a subset for temperatures between -38°C and -50°C and temperatures below -50°C, since the correlations between PLDR and the ambient temperatures show different features at different temperatures (see Figure 5). For all the cases, the histograms of cirrus PLDR follow a right-skewed distribution with a long tail extending to larger values other than a Gaussian function. In general, the PLDR values are on average larger at lower temperatures (T < -50°C) than higher temperatures. Comparisons between different years show that PLDR values at higher temperatures (-50°C < T < -38°C) are nearly the same for all the cases; while PLDR values at lower temperatures (T < -50°C) are smaller in 2020 than in the previous years with a high significance level. The altitude profiles of PLDR medians as well as the corresponding standard deviations have been further calculated for the air traffic heights between 8 and 12.3 km. The results show an increase with increasing altitudes for all the cases and PLDR values in April 2020 are nearly parallel along altitudes smaller than other years. It is reported in literature that aviation leads to the fomation of contrails and more frequent occurrence of heterogeneous freezing on aircraft exhaust particles which further leads to the formation of high-PLDR cirrus clouds. Our findings of smaller cirrus cloud occurrence rates and PLDR in 2020 caused by the reduction of air traffic are supported by this scenario.

In order to clarify the influence of air traffic reduction on the properties of cirrus clouds, the observations over China as well as over the United States of America have also been analyzed and compared with the results over Europe. Cirrus clouds observed over USA show similar properties in terms of occurrence rates and PLDR compared with Europe; while the observations over China are charaterized by smaller occurrence rates and PLDR of cirrus clouds compared with the former two regions. Besides the regional discriminations of cirrus clouds, the changes of cirrus cloud properties (PLDR) conform to the timeline of the outbreak of the coronavirus disease and the consequent restriction of air traffic in the here-compared regions.

Acknowledgements. The authors acknowledge support by the DLR-project MABAK (Innovative Methoden zur Analyse und Bewertung von Veränderungen der Atmosphäre und des Klimasystems). The work for this study has also received support from the POLDIRAD funding. We thank the NASA Langley Research Center Atmospheric Science Data Center (ASDC) and CALIPSO science team for making the data available for research.

https://doi.org/10.5194/acp-2021-172
Preprint. Discussion started: 9 March 2021

Atmospheric Chemistry and Physics Discussions

References

Ansmann, A., J. Bösenberg, A. Chaikovsky, A. Comeron, S. Eckhardt, R. Eixman, et al., Long range transport of Saharan dust to northern Europe: the 11-16 Octorber 2001 outbreak observed with EARLINET, *J. Geophys. Res.*, *108(D24)*, 4783, https://doi.org/10.1029/2003JD003757, 2003.

Bailey, M. P., and J. Hallett, Growth rates and habits of ice crystals between -20°C and -70°C, *J. Atmos. Sci.*, *61)*, 514–554, 2004.

Bailey, M. P., and J. Hallett, A comprehensive habit diagram for atmospheric ice crystals: Confirmation from the laboratory, AIRS II, and other field studies, *J. Atmos. Sci.*, *66*, 2888–2899, https://doi.org/10.1175/2009JAS2883.1, 2009.

Boucher, O., Air traffic may increase cirrus cloudiness, *Nature*, *397*, 30–31, https://doi.org/10.1038/16169, 1999.

Bühl, J., P. Seifert, A. Myagkov, and A. Ansmann, Measuring ice- and liquid-water properties in mixed-phase cloud layers at the Leipzig Cloudnet station, *Atmos. Chem. Phys.*, *16*, 10609–10620, doi:10.5194/acp-16-10609-2016, 2016.

Burton, S. P., R. A. Ferrare, M. A. Vaughan, A. H. Omar, R. R. Rogers, C. A. Hostetler, and J. W. Hair, Aerosol classification from airborne HSRL and comparisons with the CALIPSO vertical features mask, *Atmos. Meas. Tech.*, *6*, 1397–1412, doi:10.5194/amt-6-1397-2013, 2013.

Chen, J., W. B. Rossow, and Y. Zhang, Radiative effects of cloud-type variations, *J. Climate*, *13*, 264–286, 2000.

Dowling, D. R., and L. F. Radke, A summary of the physical properties of cirrus clouds, *J. Appl. Meteorol.*, *29*, 970–978, 1990.

Freudenthaler, V., M. Esselborn, M. Wiegner, B. Heese, M. Tesche, A. Ansmann, D. Müller, D. Althause, M. Wirth, A. Fix, G. Ehret, P. Knippertz, C. Toledano, J. Gasteiger, M. Garhammer, M. Seefeldner, Depolarization ratio profiling at several wavelengths in pure Saharan dust during SAMUM 2006, *Tellus*, *61B*, 165–179, 2009.

Graf, K., U. Schumann, H. Mannstein, and B. Mayer, Aviation induced diurnal North Atlantic cirrus cover cycle, *Geophys. Res. Lett.*, *39*, L16804, doi:10.1029/2012GL052590, 2012.

Groß, S., M. Tesche, V. Freudenthaler, C. Toledano, M. Wiegner, A. Ansmann, D. Althausen, and M. Seefeldner, Characterization of Saharan dust, marine aerosols and mixtures of biomass-burning aerosols and dust by means of multi-wavelength depolarization and Raman lidar measurements during SAMUM 2, *Tellus*, *63B*, 706–724, 2011.

Groß, S., V. Freudenthaler, M. Wiegner, J. Gasteiger, A. Geiß, and F. Schnell, Dual-wavelength linear depolarization ratio of volcanic aerosols: Lidar measurements of the Eyjafjallaökull plume over Maisach, Germany, *Atmos. Environ.*, *48*, 85–96, DOI: 10.1016/j.atmosenv.2011.06.017, 2012.

Haag, W. and B. Kärcher, The impact of aerosols and gravity waves on cirrus clouds at mid-latitudes, *J. Geophys. Res.*, *109*, D12202, doi:10.1029/2004JD004579, 2004.

Heymsfield, A. J., Precipitation development in stratiform ice clouds: A microphysical and dynamical study *J. Atmos. Sci.*, *34*, 367–381, 1977.

Heymsfield, A. J., Properties of tropical and midlatitude ice cloud particle ensembles. Part I: Median maass diameters and terminal velocities, *J. Atmos. Sci.*, *60*, 2573–2591, 2003.

Hunt, W. H., D. M. Winker, M. A. Vaughan, K. A. Powell, P. L. Lucker, and C. Weimer, CALIPSO lidar description and performance assessment, *J. Atmos. Oceanic Technol.*, *26*, 1214–1228, 2009.

Hu, Y., D. Winker, M. Vaughan, and Coauthors, CALIPSO/CALIOP cloud phase discrimination algorithm, *J. Atmos. Oceanic Technol.*, *26*, 2293–2309, https://doi.org/10.1175/2009JTECHA1280.1, 2009.

https://doi.org/10.5194/acp-2021-172
Preprint. Discussion started: 9 March 2021

Jensen, E. J., and O. B. Toon, The potential impact of soot particles from aircraft exhaust on cirrus clouds, *J. Geophys. Res. Lett.*, *24(3)*, 249–252, https://doi.org/10.1029/96GL03235, 1997.

Kalnay, E., and Coauthors, The NCEP/NCAR 40-year reanalysis project, *Bull. Amer. Meteor. Soc.*, *77*, 437–471, https://doi.org/10.1175/1520-0477(1996)077<0437:TNYRP>2.0.CO;2, 1996.

Kärcher, B., O. Möhler, P. J. DeMott, S. Pechtl, F. Yu, Insights into the role of soot aerosols in cirrus cloud formation, *Atmos. Chem. Phys.*, *7(16*, 4203–4227, https://doi.org/10.5194/acp-7-4203-2007, 2007.

Kärcher, B., Cirrus clouds and their response to anthropogenic activities, *Curr. Clim. Change Rep.*, *3*, 45–57, https://doi.org/10.1007/s40641-017-0060-3, 2017.

Kistler, R., E. Kalnay, and Coauthors, The NCEP/NCAR 50-year reanalysis: Monthly means CD-ROM and documentation, *Bull. Amer. Meteor. Soc.*, *82*, 247–268, https://doi.org/10.1175/1520-0477(2001)082<0247:TNNYRM>2.3.CO;2, 2001.

Khvorostyanov, V., and K. Sassen, Toward the theory of homogeneous nucleation and its parameterization for cloud models, *Geophys. Res. Lett.*, *25*, 3155–3158, 1998.

Korolev, A. V., G. A. Isaac, and J. Hallett, Ice particle habits in Arctic clouds, *Geophys. Res. Lett.*, *26*, 1299–1302, https://doi.org/10.1029/1999GL900232, 1999.

Liu, Z., M. Vaughan, D. Winker, C. Hostetler, L. Poole, D. Hlavka, W. Hart, and M. McGill, Use of probability distribution functions for discriminating between cloud and aerosol in lidar backscatter data, *J. Geophys. Res.*, *109*, D15202, doi:10.1029/2004JD004732, 2004.

Liu, Z., M. Vaughan, D. Winker, C. Kittaka, B. Getzewich, R. Kuehn, A. Omar, K. Powell, C. Trepte, and C. Hostetler, The CALIPSO lidar cloud and aerosol discrimination: Version 2 algorithm and initial assessment of performance, *J. Atmos. Oceanic Technol.*, *26*, 1198–1213, https://doi.org/10.1175/2009JTECHA1229.1, 2009.

Lopes, F. J. S., E. Landulfo, and M. A. Vaughan, Evaluating CALIPSO's 532 nm lidar ratio selection algorithm using AERONET sun photometers in Brazil, *Atmos. Meas. Tech.*, *6*, 3281–3299, doi:10.5194/amt-6-3281-2013, 2013.

Mace, G. G., M. Deng, B. Soden, and E. Zipser, Association of tropical cirrus in the 10–15-km layer with deep convective sources: An observational study combining millimeter radar data and satellite-derived trajectories, *J. Atmos. Sci.*, *63*, 480–503, doi:10.1175/JAS3627.1, 2006.

McGill, M. J., M. A. Vaughan, C. R. Trepte, W. D. Hart, D. L. Hlavka, D. M. Winker, and R. Kuehn, Airborne validation of spatial properties measured by the CALIPSO lidar, *J. Geophys. Res.*, *112*, D20201, doi:10.1029/2007JD008768, 2007.

Mamouri, R. E., V. Amiridis, A. Papayannis, E. Giannakaki, G. Tsaknakis, and D. S. Balis, Validation of CALIPSO space-borne-derived attenuated backscatter coefficient profiles using a ground-based lidar in Athens, Greece, *Atmos. Meas. Tech.*, *2*, 513–522, 2009.

Nazaryan, H., M. P. McCormick, and W. P. Menzel, Global characterization of cirrus clouds using CALIPSO data, *J. Geophys. Res.*, *113*, D16211, doi:10.1029/2007JD009481, 2008.

Noel, V., H. Chepfer, M. Haeffelin, and Y. Morille, Classification of ice crystal shapes in midlatitude ice clouds from three years of lidar observations over the SIRTA observatory, *J. Atmos. Sci.*, *63*, 2978–2991, https://doi.org/10.1175/JAS3767.1, 2006.

Omar, A., D. Winker, M. Vaughan, D. Winker, Y. Hu, and Coauthers, The CALIPSO automated aerosol classification and lidar ratio selection algorithm, *J. Atmos. Oceanic Technol.*, *26*, 1994–2014, https://doi.org/10.1175/2009JTECHA1231.1, 2009.

Pappalardo, G., U. Wandinger, L. Mona, A. Hiebsch, and et al., EARLINET correlative measurements for CALIPSO: First intercomparison results, *J. Geophys. Res.*, *115*, D00H19, doi:10.1029/2009JD012147, 2009.

Sassen, K., M. K. Griffin, and G. C. Dodd, Optical scattering and microphysical properties of subvisual cirrus clouds and climatic implications, *J. Appl. Meteorol.*, *28*, 91–98, https://doi.org/10.1175/1520-0450(1989)028<0091:OSAMPO>2.0.CO;2, 1989.

https://doi.org/10.5194/acp-2021-172
Preprint. Discussion started: 9 March 2021

Sassen, K., and S. Besson, A midlatitude cirrus cloud climatology from the facility for atmospheric remote sensing. Part II: Microphysical properties derived from lidar depolarization, *J. Atmos. Sci.*, *58*, 2103–2111, 2001.

Sassen, K., The polarization lidar technique for cloud research: A review and current assessment, *Bull. Amer. Meteor. Soc.*, *72*, 1848–1866, https://doi.org/10.1175/1520-0477(1991)072<1848:TPLTFC>2.0.CO;2, 1991.

Sassen, K., Z. Wang, and D. Liu, Global distribution of cirrus clouds from CloudSat/Cloud-Aerosol Lidar and Infrared Pathfinder Satellite Observations (CALIPSO) measurements, *J. Geophys. Res.*, *113*, D00A12, doi:10.1029/2008JD009972, 2008.

Sassen, K., and J. Zhu, A global survey of CALIPSO linear depolarization ratios in ice clouds: Initial findings, *J. Geophys. Res.*, *114*, D00H07, https://doi.org/10.1029/2009JD012279, 2009.

Schotland, R. M., K. Sassen, and R. Stone, Observations by lidar of linear depolarization ratios for hydrometeors, *J. Appl. Meteorol.*, *10*, 1011–1017, 1971.

Schumann, U., On conditions for contrail formation from aircraft exhausts, *Meteorologische Zeitschrift*, *5*, 4–23, 1996.

Schumann, U., and K. Graf, Aviation-induced cirrus and radiation changes at diurnal timescales, *J. Geophys. Res.*, *118*, 2404–2421, doi:10.1002/jgrd.50184, 2013.

Schumann, U., I. Poll, R. Teoh, R. Koelle, E. Spinielli, J. Molloy, G. S. Koudis, R. Baumann, L. Bugliaro, M. Stettler, and C. Voigt, Air traffic and contrail changes during COVID-19 over Europe: A model study, *Atmos. Chem. Phys. Discuss.*, *118*, https://doi.org/10.5194/acp-2021-62, in review, 2021.

Seifert, M., J. Ström, R. Krejci, A. Minikin, A. Petzold, J.-F. Gayet, H. Schlager, H. Ziereis, U. Schumann, and J. Ovarlez, *Atmos. Chem. Phys.*, *4*, 1343–1353, 2004.

Stephens, G. L., S-C. Tsay, P. W. Stackhouse Jr., and P. J. Flatau, The relevance of the microphysical and radiative properties of cirrus clouds to climate and climatic feedback, *J. Atmos. Sci.*, *47*, 1742–1754, 1990.

Stephens, G., D. M. Winker, J. Pelon, C. Trepte, D. Vane, C. Yuhas, T. L'Ecuyer, and M. Lebsock, CloudSat and CALIPSO within the A-Train: Ten years of actively observing the Earth system, *Bull. Amer. Meteor. Soc.*, *99*, 569–581, https://doi.org/10.1175/BAMS-D-16-0324.1, 2018.

Stettler, M. E., A. M. Boies, A. Petzold, and S. R. Barrett, Global civil aviation black carbon emissions, *Environ. Sci. Technol.*, *47*, 10397–10404, https://doi.org/10.1021/es401356v, 2013.

Ström, J., and S. Ohlsson, In situ measurements of enhanced crystal number densities in cirrus clouds caused by aircraft exhaust, *J. Geophys. Res.*, *103*, 11355–11361, 1998.

Takano, Y., and K. N. Liou, Solar radiative transfer in cirrus clouds. Part I: Single-scattering and optical properties of hexagonal ice crystals, *J. Atmos. Sci.*, *46*, 3–19, https://doi.org/10.1175/1520-0469(1989)046<0003:SRTICC>2.0.CO;2, 1989.

Tesche, M., A. Ansmann, D. Müller, D. Althausen, R. Engelmann, V. Freudenthaler, and S. Groß, Vertically resolved separation of dust and smoke over Cape Verde using multi-wavelength Raman and polarization lidars during Saharan Mineral Dust Experiment 2008, *J. Geophys. Res.*, *114*, D13202, doi:10.1029/2009JD011862, 2009.

Tesche, M., P. Achtert, P. Glantz, K. J. Noone, Aviation effects on already-existing cirrus clouds, *Nat. Commun.*, *7(1)*, 12016, https://doi.org/10.1038/ncomms12026, 2018.

Um, J., G. M. McFarquhar, Y. P. Hong, S.S. Lee, C. H. Jung, R. P. Lawson, and Q. Mo, Dimensions and aspect ratios of natural ice crystals, *Atmos. Chem. Phys.*, *15*, 3933–3956, https://doi.org/10.5194/acp-15-3933-2015, 2015.

Urbanek, B., S. Groß, M. Wirth, C. Rolf, M. Krämer, and C. Voigt, High depolarization ratios of naturally occurring cirrus clouds near air traffic regions over Europe, *Geophys. Res. Lett.*, *45*, 13,166–13,172, https://doi.org/10.1029/2018GL079345, 2018.

https://doi.org/10.5194/acp-2021-172
Preprint. Discussion started: 9 March 2021

Vaughan, M. A., K. A. Powell, R. E. Kuehn, S. A. Young, D. M. Winker, C. A. Hostetler, W. H. Hunt, Z. Liu, M. J. McJill, and B. J. Getzewich, Fully automated detection of cloud and aerosol layers in the CALIPSO lidar measurements, *j. Atmos. Oceanic Technol.*, *26*, 2034–2050, https://doi.org/10.1175/2009JTECHA1228.1, 2009.

Voigt, C., U. Schumann, P. Jessberger, T. Jurkat, A. Petzold, J.-F. Gayet, M. Krämer, T. Thornberry, and D. W. Fahey, Extinction and optical depth of contrails, *Geophys. Res. Lett.*, *38*, L11806, doi:10.1029/2011GL047189, 2011.

Voigt, C., U. Schumann, and Coauthors, ML-CIRRUS: The airborne experiment on natural cirrus and contrail cirrus with the high-altitude long-range research aircraft HALO, *Bull. Amer. Meteor. Soc.*, *98*, 271–288, https://doi.org/10.1175/BAMS-D-15-00213.1, 2017.

Winker, D. M., M. A. Vaughan, A. Omar, Y. Hu, and K. A. Powell, Overview of the CALIPSO mission and CALIOP data processing algorithms, *j. Atmos. Oceanic Technol.*, *26*, 2310–2323, https://doi.org/10.1175/2009JTECHA1281.1, 2009.

Winker, D. M., and Coauthors, The CALIPSO Mission: A global 3D view of aerosols and clouds, *Bull. Amer. Meteor. Soc.*, *91*, 1211–1229, https://doi.org/10.1175/2010BAMS3009.1, 2010.

Winker, D. M., B. H. Hunt, and M. J. McGill, Initial performance assessment of CALIOP, *Geophys. Res. Lett.*, *34*, L19803, doi:10.1029/2007GL030135, 2007.

https://doi.org/10.5194/acp-2021-172
Preprint. Discussion started: 9 March 2021

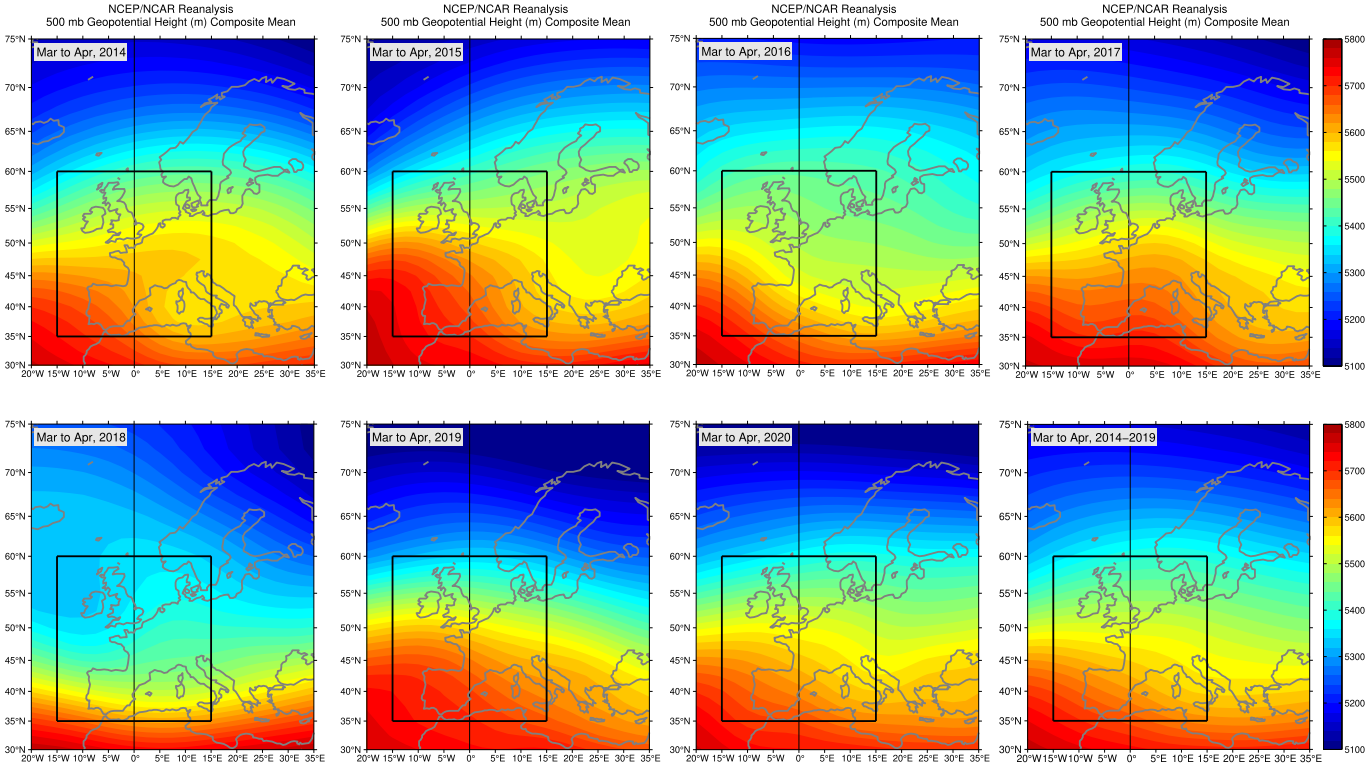

Figure 1. 500-mb geopotential height composite mean in March and April for years 2014-2020 (with years indicated on the plot) and for the average in the previous years 2014-2019 (Rightmost-bottom panel) over Europe. The black boxes indicate the research area of this manuscript. The plots are reproduced based on NCEP/NCAR Reanalysis provided by Physical Sciences Laboratory, NOAA, Boulder, Colorado, from their their Web site at https://psl.noaa.gov/.

https://doi.org/10.5194/acp-2021-172
Preprint. Discussion started: 9 March 2021

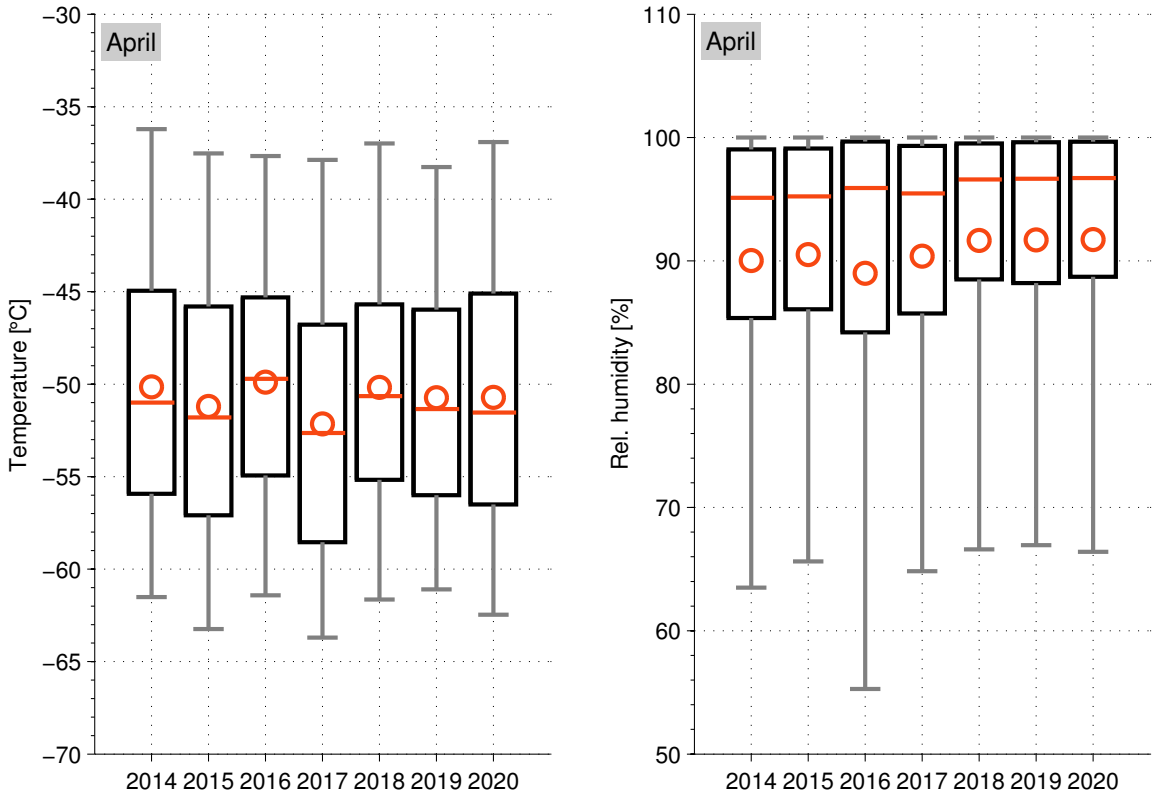

Figure 2. Boxplots of background temperature and relative humidity along with their median (red solid lines) and mean (red circles) values in April over Europe within the altitude range between 8 and 13 km. Black boxes stand for 25th–75th percentiles (top and bottom) and whiskers in grey for the 5th and 95th percentiles. The data are directly derived from the GEOS-5 model data product provided to the CALIPSO files by the GMAO data assimilation system.

https://doi.org/10.5194/acp-2021-172
Preprint. Discussion started: 9 March 2021

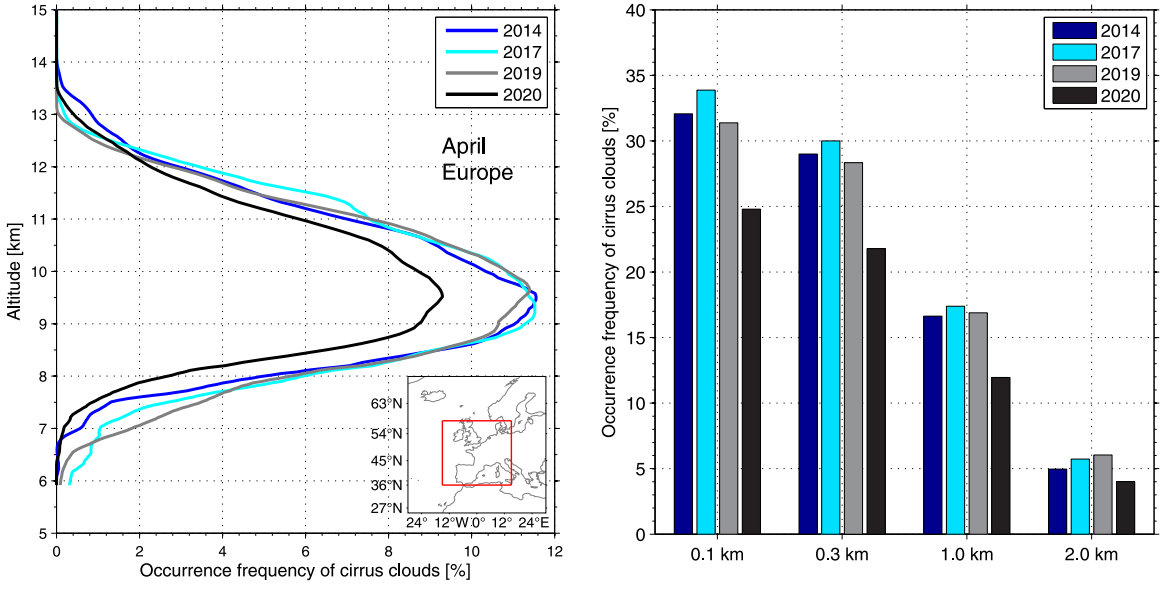

Figure 3. Occurrence rates of cirrus clouds derived from the lidar measurements of CALIPSO in April in different years 2014, 2017, 2019, and 2020. Only observations of cirrus clouds at temperatures below -38°C, at altitudes above 6 km and with cloud thickness larger than 0.1 km are analyzed. Location of research area where cirrus clouds were detected is shown on the map (Latitude: 35°N–60°N; Longitude: 15°W–15°E). Left panel: Altitude profiles of cirrus occurrence rates (mean values); Right panel: Histograms of the cirrus occurrence ratios with the definitions based on different cloud thicknesses, respectively.

https://doi.org/10.5194/acp-2021-172
Preprint. Discussion started: 9 March 2021

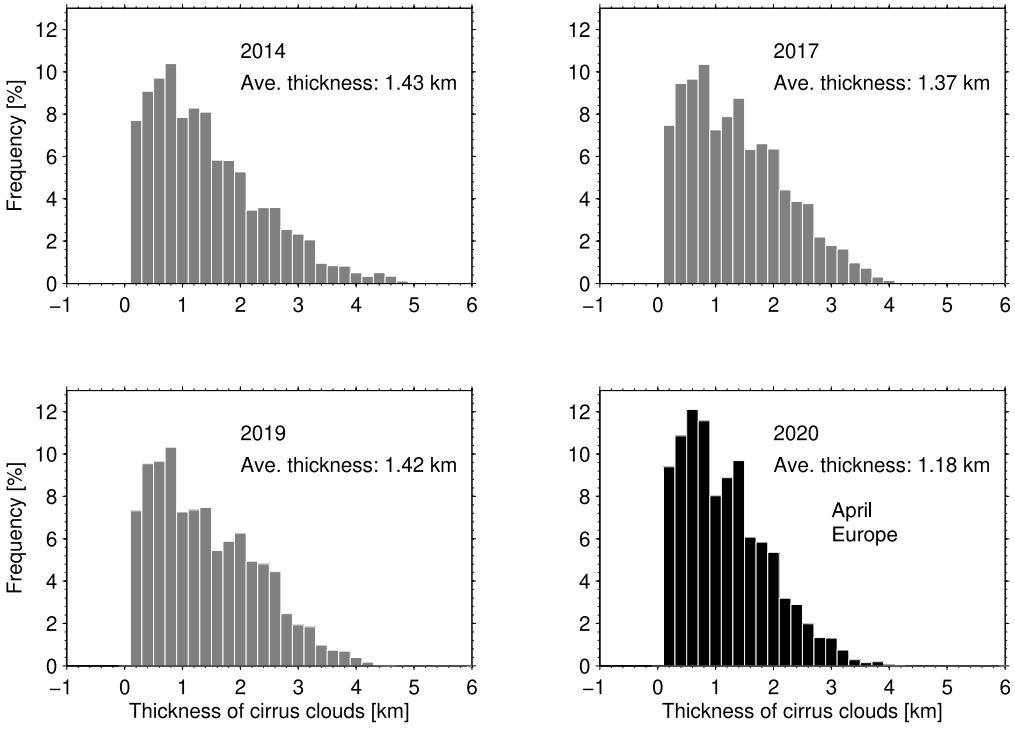

Figure 4. Histograms of cirrus cloud thicknesses in April in 2020 (Right-bottom panel) compared with the reference years. The average cloud thicknesses in different years are indicated on the corresponding panels.

https://doi.org/10.5194/acp-2021-172
Preprint. Discussion started: 9 March 2021

Atmospheric Chemistry and Physics Discussions

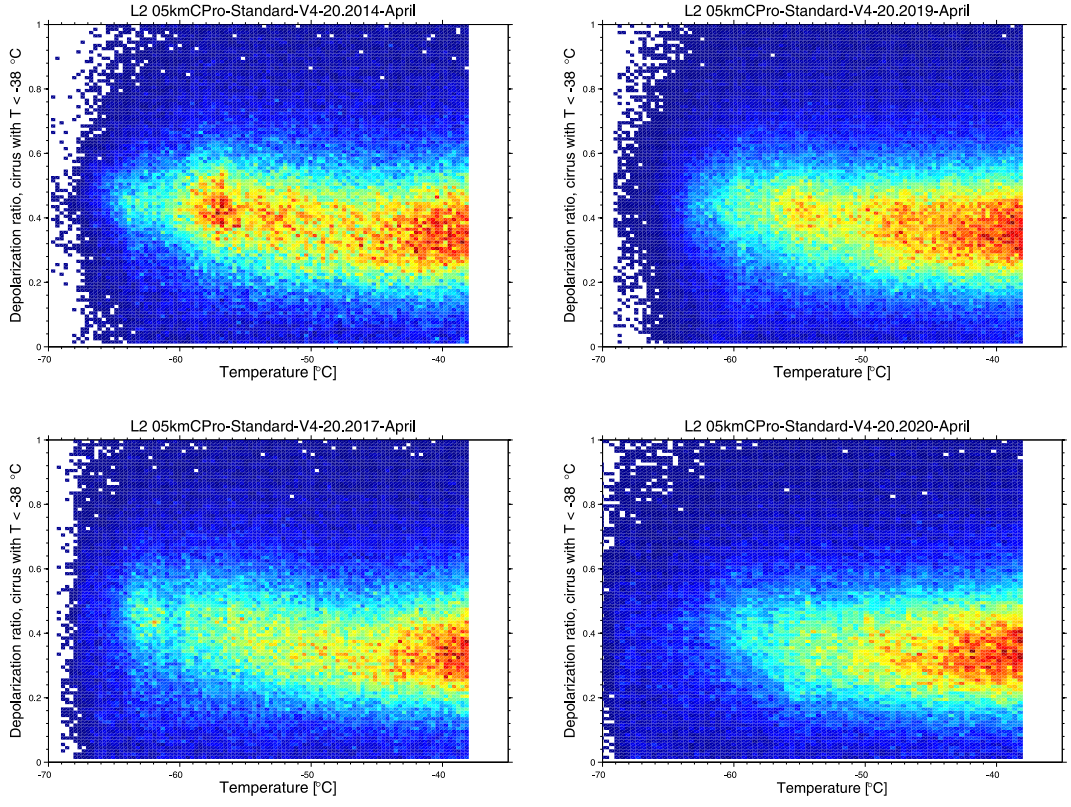

Figure 5. Correlations between the particle linear depolarization ratios (PLDR) of cirrus clouds and the ambient temperatures derived from the lidar measurements of CALIPSO and GEOS-5 model data, respectively. The color codes are used to visualize the number densities of scatter point data: more red area indicating larger number densities.

https://doi.org/10.5194/acp-2021-172
Preprint. Discussion started: 9 March 2021

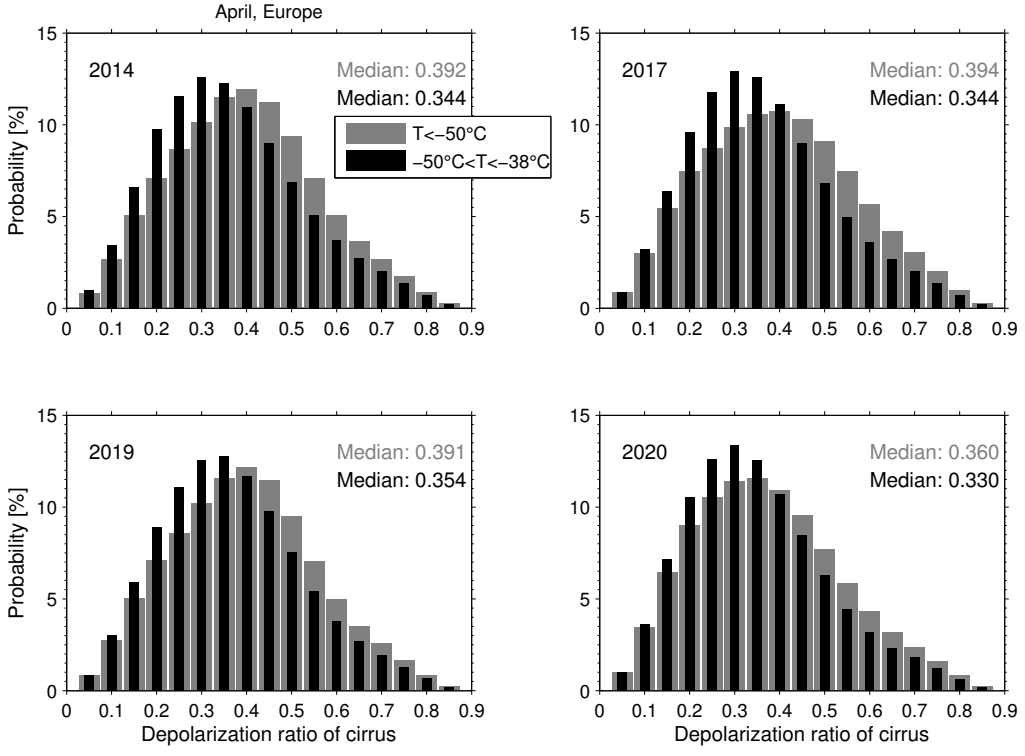

Figure 6. Distibutions of the PLDR of cirrus clouds detected at temperatures from -50°C to -38°C (black) and at temperatures colder than -50°C (grey). The corresponding medians for each case are indicated on the plot.

https://doi.org/10.5194/acp-2021-172
Preprint. Discussion started: 9 March 2021

Atmospheric Chemistry and Physics Discussions

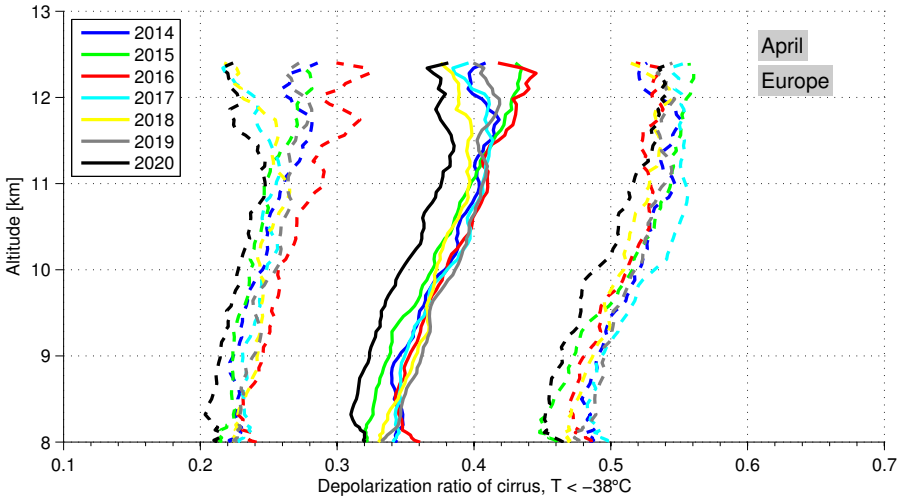

Figure 7. Altitude profiles of the medians of cirrus PLDR (solid lines) and their corresponding 20% and 80% percentiles derived from the CALIPSO observations in April at temperatures below -38°C within the altitude range between 8 and 12.3 km. For all the profiles, resulting PLDR medians show in general an increase with increasing altitudes.

https://doi.org/10.5194/acp-2021-172
Preprint. Discussion started: 9 March 2021

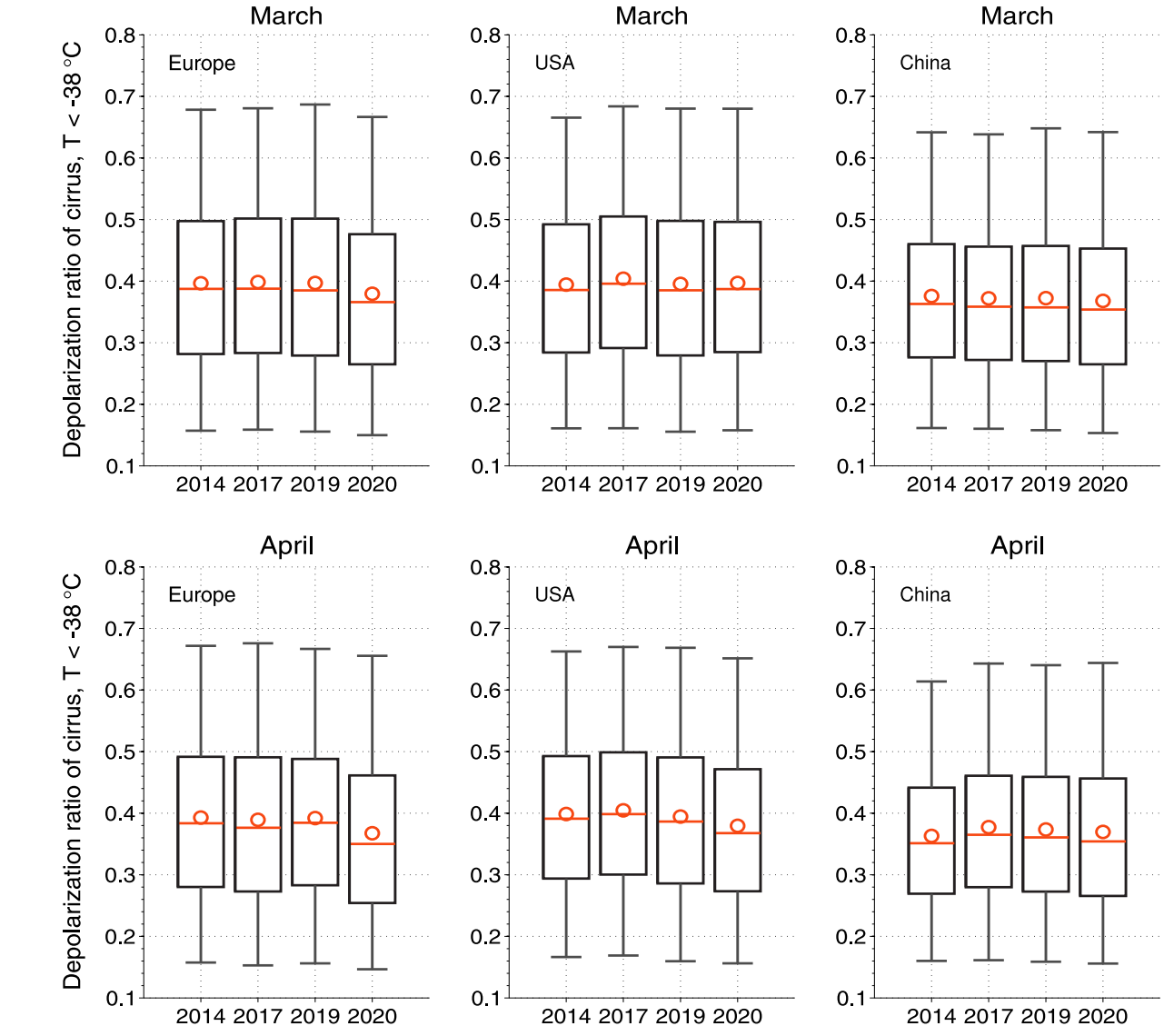

Figure 8. Boxplot representations of the PLDR of cirrus clouds detected in different years over Europe (left panels), the United States of America (middle panels), and China (right panels). Upper panels for the observations in March; Lower panels for April. Boxes represent 25th–75th percentiles (top and bottom) and the solid lines in red through the corresponding boxes stand for the medians and red circles for means; whiskers in grey indicate the 5th and 95th percentiles and outliers which are larger than the upper whisker or smaller than the lower whisker are not shown here.